Electronic structure and magneto-optical spectra of La$_x$Sr$_{1-x}$MnO$_3$ perovskites: Theory and experiment

L. Uba,[1] S. Uba,[1] L. P. Germash,[2] L. V. Bekenov,[3] and V. N. Antonov[3,4]

[1]*Institute of Computer Science, University of Bialystok, Lipowa 41, PL-15-424 Bialystok, Poland*
[2]*National Technical University of Ukraine, Kiev Polytechnical Institute 14 Politehnichna Street, 03056 Kiev, Ukraine*
[3]*Institute of Metal Physics, Vernadsky Street, 03142 Kiev, Ukraine*
[4]*Max-Planck-Institut für Festkörperforschung, Heisenberg Strasse 1, D-70569 Stuttgart, Germany*

The electronic structure and optical and magneto-optical Kerr (MOKE) spectra of La$_x$Sr$_{1-x}$MnO$_3$ ($x = 0.0$, 0.25) perovskites have been investigated experimentally and theoretically from first principles, using the fully relativistic Dirac linear MT-orbital band structure method in the local spin density approximation (LSDA) as well as within the LSDA $+ U$ approach. It is shown that the *ab initio* calculations reproduce well the experimental spectra and make it possible to explain the microscopic origin of the LaMnO$_3$ and La$_{0.75}$Sr$_{0.25}$MnO$_3$ optical and magneto-optical response in terms of interband transitions. We found that the electrons in close vicinity to the Fermi level are strongly correlated. To produce the correct energy gap in the LaMnO$_3$ or right value of electron polarization at the Fermi level in ferromagnetic metallic La$_{1-x}$Sr$_x$MnO$_3$ doped alloys one has to take into account strong Coulomb correlations. On the other hand, the electronic structure and optical and MOKE spectra can be described satisfactorily in terms of LSDA energy bands in a wide energy range beyond close vicinity of the Fermi level. The Coulomb correlations are reduced in transition from the LaMnO$_3$ to the La$_{1-x}$Sr$_x$MnO$_3$.

I. INTRODUCTION

Transition-metal perovskites have been studied for half a century, and most intensively during the last decade, for their fascinating electronic and magnetic properties arising from narrow 3d bands and strong Coulomb correlations.[1–5] Recently, considerable experimental and theoretical efforts have been devoted to the study of perovskite manganites with general formula $R_x A_{1-x}$MnO$_3$ ($0 \leqslant x \leqslant 1$), where R is a rare-earth atom (e.g., La, Pr, Nd) and A is an alkali-metal atom (e.g., Ca, Sr, Ba).[6] These materials exhibit puzzling physical properties related to a complex interplay between orbital, magnetic, charge, and structural degrees of freedom. They include colossal-magnetoresistance (CMR) effect and a large variety of phases with remarkably different structural, magnetic, and transport properties.[7–9]

Among the manganese oxides, LaMnO$_3$ (LMO) is important because it is the parent system in the family of manganites that show the CMR effect. At ambient conditions LMO is an insulator with orthorhombic perovskite structure (space group $Pbnm$).[10–12] Alternating long and short Mn-O distances in the ac plane of the structure is a sign of orbital ordering which arises from a cooperative Jahn-Teller (JT) distortion. The latter removes the degeneracy of the e_g orbitals in the $t_{2g}^3 e_g^1$ electron configuration of the Mn^{3+} ions and stabilizes the $3d_{3z^2-r^2}$ with respect to the $3d_{x^2-y^2}$ orbitals. It is the origin of so-called A-type antiferromagnetism below $T_N = 140$ K, in which spins align parallel in the xy plane and antiparallel along the z direction.[13,14]

There has been intense discussion about the primary cause of the insulating ground state of LMO.[15–19] In one interpretation LMO is regarded, like many insulating transition-metal oxides, as a Mott-type (or charge-transfer) insulator; that is, the electrical properties are dominated by electron-electron interactions leading to a localization of the e_g conduction electrons. On the other hand, Millis *et al.* concluded that

the insulating behavior of the paramagnetic phase cannot be explained by a purely electronic model.[16,17] Strong JT electron-phonon coupling was proposed as the crucial component which localizes the e_g electrons as polarons.

Doped LaMnO$_3$ systems with divalent cations such as Ca, Sr, or Ba have attracted recent attention since the discovery of CMR phenomena in La$_{1-x}$Ca$_x$MnO$_3$ (LCMO) near room temperature.[20] As the nominal hole concentration (x) is increased, La$_{1-x}$Sr$_x$MnO$_3$ (LSMO) shows a phase change from an antiferromagnetic to a ferromagnetic state around $x = 0.1$, and subsequently the low-temperature ferromagnetic phase undergoes an insulator-to-metal transition around $x = 0.17$.[1,2,21] Such a conducting ferromagnetic state is explained by the double-exchange mechanism.[22,23] In the metallic phase, the conduction band consists of 3d e_g states hybridized strongly with the O 2p states, while the t_{2g} electrons are still localized.

In this work we focus our attention on the experimental and theoretical investigation of the optical and MO properties of LaMnO$_3$ and La$_{1-x}$Sr$_x$MnO$_3$ compounds. The optical spectra of LMO and LSMO were quite well investigated experimentally by several authors;[24–32] however, the experimental data and their interpretations are varied. Tobe *et al.*[29] investigated anisotropic optical conductivity spectra over a wide temperature range for a single crystal of LMO. The charge-gap transition peak around 2 eV shows a clear anisotropy for the polarizations parallel and perpendicular to the c axis. With the increase of temperature, the anisotropy and the gap magnitude are gradually suppressed. Optical conductivity and reflectivity spectra and their variation with temperature and doping level x have been investigated for single crystals of La$_{1-x}$Sr$_x$MnO$_3$ ($0 \leqslant x \leqslant 0.3$) by Okimoto *et al.*[26] The measured optical conductivity spectra show that La$_{1-x}$Sr$_x$MnO$_3$ with $x = 0.1$ is insulating even below T_c, for $x = 0.175$ is barely metallic below T_c but semiconducting above T_c, and for $x = 0.3$ is

metallic. Kovaleva *et al.*[32] presented a comprehensive ellipsometric study of an untwinned, nearly stoichiometric LaMnO$_3$ crystal in the spectral range $1.2-6.0$ eV at temperatures $20 \leqslant T \leqslant 300$ K. The optical complex dielectric function of single-crystalline samples of RMnO$_3$ ($R =$ La, Pr, Nd, Sm, Eu) was measured by Moskvin *et al.*[30] using ellipsometric technique at room temperature in the spectral range from 1.0 to 5.0 eV for two light polarizations: **E** $\parallel$ *c* and **E** $\perp$ *c*. Starting with a simple cluster model approach authors addressed both the one-center ($p - d$) and the two-center ($d - d$) charge-transfer (CT) transitions, their polarization properties, the role played by structural parameters, orbital mixing, and the spin degree of freedom.

Magneto-optical spectroscopy combined with spectroscopic ellipsometry offers an opportunity to learn about the transitions involving the electrons related to Mn^{3+}, Mn^{4+}, and O^{2-} ions. There were only a few previous studies of MO Kerr spectroscopy of La$_{1-x}$A$_x$MnO$_3$. Fumagalli *et al.*[33] investigated 150-nm-thick films deposited by laser ablation. Yamaguchi *et al.*[34] and Pompa and Kamminga[35] investigated bulk materials. The photoinduced effect in a ferromagnetic perovskite La$_{0.6}$M$_{0.4}$MnO$_3$ was investigated by femtosecond spectroscopy by Ogasawara *et al.* in Ref. [36]. Optical absorption and transverse Kerr effect spectra, resistivity, and magnetoresistance of La$_{1-x}$Sr$_x$CoO$_3$ ($x = 0.15$, 0.25, 0.35) films have been studied by Loshkareva *et al.*[37] Koubaa *et al.*[38] report on the strain effects upon the magneto-optical properties of La$_{2/3}$Sr$_{1/3}$MnO$_3$ thin films. Rauer *et al.*[39] investigate the ferromagnetic phase of thin epitaxial films of the manganites La$_{0.7}$Ca$_{0.3}$MnO$_3$ and La$_{0.7}$Sr$_{0.3}$MnO$_3$ by temperature-dependent spectral generalized magneto-optical ellipsometry (SGME). The measurements covering a spectral range of 0.5 to 5 eV are performed in the temperature range of 25 to 425 K. SGME allows a complete magneto-optical characterization consisting of the determination of the diagonal components ε_{xx} as well as the off-diagonal components ε_{xy} of the dielectric tensor within a single measurement. Unfortunately, they do not present the MO Kerr spectra. Magneto-optical spectroscopy combined with spectroscopic ellipsometry has been used to learn about the electronic transitions in La$_{2/3}$Sr$_{1/3}$MnO$_3$ film pulse laser deposited onto SrTiO$_3$ (STO) substrates.[40] The dispersion function of LSMO films was parameterized by the sum of three damped Lorentz oscillators and adjusted together with the film thickness numerically. With the knowledge of film optical properties the off-diagonal elements of the LSMO permittivity tensor (magneto-optical constants) were calculated from the complex polar Kerr effect measured on the thickest 60-nm LSMO film considered as optically thick.

A number of theoretical works on LaMnO$_3$ based on the density functional theory (DFT) were published during the last decade.[41–60] Roughly speaking, all the calculations may be divided into two groups. The first group suggests that the correlation effects are not significant in LMO and many aspects of the ground-state as well as single-electron excited-state properties of LMO and related compounds can be described satisfactorily in terms of local spin density approximation (LSDA) energy bands.[41–47] The second group indicates the dominant importance of the correlation effects in LMO, arguing that to get the correct experimental ground state

for LMO one has to take into account strong onsite Coulomb interactions.[48–60]

Pickett and Singh[42] have used the linearized augmented plane-wave (LAPW) method for the distorted LMO caused by the JT effect and obtained a gap of 0.12 eV for the *A*-type antiferromagnet. It seems that the LSDA itself worked well to account for the antiferromagnetic insulating ground state after including the JT distortion. Authors indicated that the failure of the LSDA method generally occurred toward the right end of the 3*d* transition-metal series, while for Mn, which is in the middle of 3*d* series, no strong correlation interaction would be expected. Density-functional calculations also show strong couplings between lattice distortions, magnetic order, and electronic properties of LMO. In particular, it is found that without lattice distortions LMO would have a *F* metallic ground state, and even if forced to be *A*-type antiferromagnetic ($A - AF$), it would still be metallic.[42] In their band studies of perovskites LaMO$_3$ ($M =$ Mn, Fe, Co, Ni), Sarma *et al.*[41] also found that the JT distortion around Mn ions was important to account for a stable *A*-type antiferromagnetic structure, which is quite different from the other three compounds ($M =$ Fe, Co, Ni). They also made the point that the electron-electron correlations are unimportant due to the relatively large hopping parameter *t* and large screening effect. Ravindran *et al.*[44] suggest that the correlation effects are not significant in LMO and the presence of ferromagnetic coupling within the *ab* plane as well as the antiferromagnetic coupling perpendicular to this plane can be explained through the itinerant band picture. The calculations based on the generalized-gradient-corrected relativistic full-potential LAPW method[44] were able to describe the electronic structure, magnetism, and the excited-state properties such as the optical spectra, x-ray photoemission, bremsstrahlung isochromat, and x-ray absorption near-edge structure spectra of LMO in good agreement with the experimental data.

On the other hand, several authors stress the dominant importance of the correlation effects in the LMO. Geng *et al.*[61] indicated that although the effects of JT distortion play a main role in getting the correct ground state in LMO, a reasonable strong electron correlation correction is necessary for obtaining the exact band structure and 3.5 eV is a good choice for the on-site Coulomb parameter *U*. Hashimoto *et al.*[57] also show that if internal coordinates and lattice constants are optimized, generalized gradient approximation (GGA) calculations fail to predict the experimental ground state with *A*-type antiferromagnetic ordering, while GGA $+ U$ calculations reproduce the experimental JT distortion and the $A - AF$ ground state successfully. The calculations for LaTiO$_3$ by Solovyev *et al.*[49] showed that the correlation correction was significant for Ti, V, and Co but less important for Mn. However, in that study the calculated intensity of the optical conductivity was found to be much smaller than the experimental results in the whole energy range. Hu *et al.*[51] reported that to get the correct experimental ground state for LMO, it is necessary to take JT distortion, electron-electron correlation, and AF ordering simultaneously into consideration. Held and Vollhardt,[62] using the dynamical mean-field theory (DMFT), emphasize the importance of electronic correlations due to the local Coulomb repulsion for understanding the properties of manganites. Maezono *et al.*[58] pointed out that the electron correlations remain strong

even in the metallic state of doped manganites. Ma *et al.*[52] investigated strain effects in LSMO using full potential linear augmented plane wave (FPLAPW) method in the GGA + U approximation. However, they used simplified tetrahedral unit cell instead of real rhombohedral one.

Some authors[53–55] indicate the importance of dynamical screening effect for the correct description of the ground state of pure and doped LMO. They used a so-called GW approximation,[63] a novel method beyond the local spin density approximation. Nohara with coauthors[55] argue that it is important to treat large on-site Coulomb interactions as well as the dynamical screening effects. They used $U + $ GW approximation to investigate electronic structures of LaMO$_3$. Transition-metal (TM) ions in perovskite-type lanthanum oxides are trivalent and their physics is qualitatively different from that of divalent TM ions in TM mono-oxides. The localization of wave functions of La $4f$ and $3d$ orbitals of TM is crucial. On the other hand, the screening effect for $3d$ orbitals is strong enough so as to reduce the on-site static-screened Coulomb interaction in trivalent oxides.

The aim of this work is the detailed experimental and theoretical investigations of the electronic structure and optical and MO properties of LaMnO$_3$ and La$_{1-x}$Sr$_x$MnO$_3$ compounds. We use in our calculations the fully relativistic Dirac LMTO band structure method. Some preliminary results of experimentally measured magneto-optical Kerr (MOKE) spectra of La$_{0.7}$A$_{0.3}$MnO$_3$ ($A = $ Sr, Ca, and Ce) were published earlier in our paper.[64]

This paper is organized as follows. Section II presents a description of the La$_{1-x}$Sr$_x$MnO$_3$ ($x = 0.0$, 0.25) crystal structures and the experimental and the computational details. Section III is devoted to experimental measurements of the MO Kerr spectra and theoretical calculations of the electronic structure and the optical and MO spectra using the fully relativistic Dirac LMTO band structure method. Theoretically calculated spectra are compared with those measured experimentally. Finally, the results are summarized in Sec. IV.

II. EXPERIMENTAL AND COMPUTATIONAL DETAILS

Magneto-optical effects refer to various changes in the polarization state of light upon interaction with materials possessing a net magnetic moment, including rotation of the plane of linearly polarized light (Faraday, Kerr rotation), and the complementary differential absorption of left and right circularly polarized light (circular dichroism). In the visible spectral range these effects result from excitation of electrons in the conduction band. Near x-ray absorption edges, or resonances, magneto-optical effects can be enhanced by transitions from well-defined atomic core levels to transition symmetry selected valence states. Using straightforward symmetry considerations it can be shown that all MO phenomena are caused by the symmetry reduction, in comparison to the paramagnetic state, caused by magnetic ordering.[65] Concerning optical properties this symmetry reduction only has consequences when spin-orbit (SO) coupling is considered in addition. To calculate MO properties one therefore has to account for magnetism and SO coupling at the same time when dealing with the electronic structure of the material considered.

For the polar Kerr magnetization geometry and a crystal of tetragonal symmetry, where both the fourfold axis and the magnetization **M** are perpendicular to the sample surface and the z axis is chosen to be parallel to them, the dielectric tensor is composed of the diagonal ε_{xx} and ε_{zz}, and the off-diagonal ε_{xy} components in the form

$$\boldsymbol{\varepsilon} = \begin{pmatrix} \varepsilon_{xx} & \varepsilon_{xy} & 0 \\ -\varepsilon_{xy} & \varepsilon_{xx} & 0 \\ 0 & 0 & \varepsilon_{zz} \end{pmatrix}. \tag{1}$$

The various elements $\hat{\varepsilon}_{\alpha\beta}$ are composed of real and imaginary parts as follows: $\hat{\varepsilon}_{\alpha\beta} = \varepsilon_{\alpha\beta}^{(1)} + i\varepsilon_{\alpha\beta}^{(2)}$, where $\alpha, \beta \equiv x, y, z$, $\varepsilon_{xx} = (n + ik)^2$, and n and k are refractive index and extinction coefficient, respectively. The optical conductivity tensor $\hat{\sigma}_{\alpha\beta} = \sigma_{\alpha\beta}^{(1)} + i\sigma_{\alpha\beta}^{(2)}$ is related to the dielectric tensor $\varepsilon_{\alpha\beta}$ through the equation

$$\hat{\varepsilon}_{\alpha\beta}(\omega) = \delta_{\alpha\beta} + \frac{4\pi i}{\omega}\hat{\sigma}_{\alpha\beta}(\omega). \tag{2}$$

A complete description of MO effects in this formalism is given by the four nonzero elements of the dielectric tensor or, equivalently, by the complex refractive index $\hat{N}(\omega)$,

$$\hat{N}(\omega) \equiv \sqrt{\hat{\varepsilon}(\omega)} = n(\omega) + ik(\omega), \tag{3}$$

for several normal modes corresponding to the propagation of pure polarization states along specific directions in the sample. The solution of Maxwell's equations yields these normal modes.[66] One of these modes is for circular components of opposite ($\pm$) helicity with the wave vector **q** $\parallel$ **M** having indexes

$$\hat{N}_{\pm} = n_{\pm} + ik_{\pm} = \sqrt{\varepsilon_{xx} \pm i\varepsilon_{xy}}. \tag{4}$$

The two other cases are for linear polarization with **q** $\perp$ **M**.[67] One has the electric vector **E** $\parallel$ **M** and index $\hat{N}_{\parallel} = n_{\parallel} + ik_{\parallel} = \sqrt{\varepsilon_{zz}}$. The other has **E** $\perp$ **M** and $\hat{N}_{\perp} = n_{\perp} + ik_{\perp} = \sqrt{(\varepsilon_{xx}^2 + \varepsilon_{xy}^2)/\varepsilon_{xx}}$.

At normal light incidence the relation between the polar complex Kerr angle and the dielectric tensor components is given by[68]

$$\frac{1 + \tan\eta}{1 - \tan\eta}e^{2i\theta} = \frac{1 + \hat{N}_+}{1 - \hat{N}_+}\frac{1 - \hat{N}_-}{1 + \hat{N}_-}, \tag{5}$$

where θ and η are the polar Kerr rotation and the ellipticity, respectively. From Eq. (5) it can be seen that the maximal observable rotation θ is $\pm 90°$ and maximal achievable Kerr ellipticity η is $\pm 45°$.

The Kerr rotation and ellipticity are for most materials less than $1°$. The above exact expression can be approximated for small θ and η by the expression[69]

$$\theta + i\eta \approx \frac{-\varepsilon_{xy}}{(\varepsilon_{xx} - 1)\sqrt{\varepsilon_{xx}}}. \tag{6}$$

The optical conductivity of LMO and LMSO has been computed from the energy bandstructure by means of the

Kubo-Greenwood[70] linear-response expression:[71]

$$\sigma_{\alpha\beta}(\omega)$$
$$= \frac{-ie^2}{m^2\hbar V_{uc}} \sum_{\mathbf{k}} \sum_{nn'} \frac{f(\epsilon_{n\mathbf{k}}) - f(\epsilon_{n'\mathbf{k}})}{\omega_{nn'}(\mathbf{k})} \frac{\Pi^{\alpha}_{n'n}(\mathbf{k})\Pi^{\beta}_{nn'}(\mathbf{k})}{\omega - \omega_{nn'}(\mathbf{k}) + i\gamma},$$

$$(7)$$

where $f(\epsilon_{n\mathbf{k}})$ is the Fermi function, $\hbar\omega_{nn'}(\mathbf{k}) \equiv \epsilon_{n\mathbf{k}} - \epsilon_{n'\mathbf{k}}$ is the energy difference of the Kohn-Sham energies, and γ is the lifetime parameter, which is included to describe the finite lifetime of the excited Bloch electron states. The $\Pi^{\alpha}_{nn'}$ are the dipole optical transition matrix elements, which in a fully relativistic description are given by

$$\mathbf{\Pi}_{nn'}(\mathbf{k}) = \langle \psi_{n\mathbf{k}} | c\boldsymbol{\alpha} | \psi_{n'\mathbf{k}} \rangle, \qquad (8)$$

with the four-component Bloch electron wave function $\psi_{n\mathbf{k}}$, velocity of light c, and Dirac operator $\boldsymbol{\alpha}$. The combined correction terms were also taken into account in the optical matrix element calculations. The detailed description of the optical matrix elements in the Dirac representation is given in Refs. 72 and 73. Last, we mention that the absorptive part of the optical conductivity was calculated in a wide energy range and than the Kramers-Kronig transformation was used to calculate the dispersive parts of the optical conductivity from the absorptive ones. For the interband relaxation parameter we used the value $\gamma = 0.6$ eV.

The details of the computational method are described in our previous papers,[74–77] and here we only mention several aspects. The calculations were performed for the experimentally observed lattice constants using the spin-polarized fully relativistic linear-muffin-tin-orbital (SPR LMTO) method[78,79] in the atomic sphere approximation (ASA) with the combined correction term taken into account. The LSDA part of the calculations was based on the spin-density functional with the von Barth-Hedin parametrization[80] of the exchange-correlation potential. Brillouin zone (BZ) integrations were performed using the improved tetrahedron method[81] and charge self-consistently was obtained on a grid of 729 and 417 points in the irreducible part of the BZ of LMO and LSMO, respectively. To improve the potential we include an additional empty spheres in the vacancy sites. The basis consisted of La, Mn, Sr s, p, d, and f; O s, p, and d and empty sphere s, and p LMTO's. The radii of atomic spheres are equal to 3.194, 2.412, 1.938, and 1.894 a.u. for the La, Mn, O_1, and O_2, respectively. We have adopted the LSDA + U method[82] as a different level of approximation to treat the electron-electron correlations. We used the rotationally invariant LSDA + U method. This method is described in detail in our previous paper.[83] The effective on-site Coulomb repulsion U was considered as an adjustable parameter. For the exchange integral J the value of 0.92 eV estimated from constrained LSDA calculations was used.

LaMnO$_3$ compound crystallizes in the orthorhombic GdFeO$_3$-type structure[84] containing four formula units (space group $Pbnm$, No. 62) as shown in Fig. 1. The structural parameters used in the calculations are equal to[85] $a = 5.2337$ Å, $b = 5.4044$ Å, and $c = 7.2801$ Å and atom positions La in 4c $(-0.00714\ 0.04803\ 0.25)$, Mn in 4$a$ $(0.5\ 0\ 0)$, O_1 in 4c $(0.42929\ 0.00975\ 0.25)$, and O_2 in 8d $(0.22579\ 0.1999\ -0.03194)$.
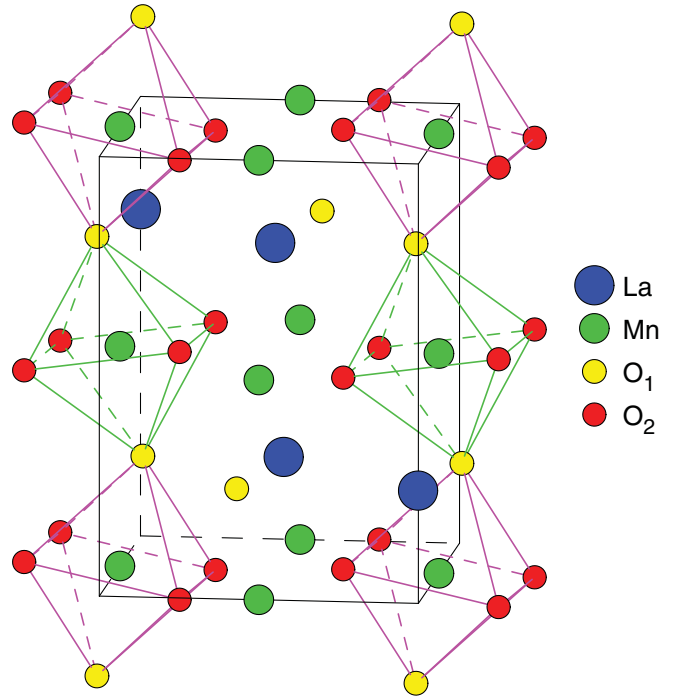

FIG. 1. (Color online) Schematic representation of the orthorhombic GdFeO$_3$-type crystal structure of LaMnO$_3$.

Basically, two different types of distortions are included in the structure shown in Fig. 1. One is a tilting of the MnO$_6$ octahedra around the cubic [110] axis as in GdFeO$_3$ so that the Mn-O-Mn angle changes from $180°$ to $\sim160°$. The second type of crystal distortion in LaMnO$_3$ is the deformation of the MnO$_6$ octahedra caused by the JT effect, viz., originating from orbital degeneracy. This may be looked upon as a cooperative shifting of the oxygens within the ab plane away from one of its two nearest-neighboring Mn atoms toward the others, thus creating long and short Mn-O bond lengths (modified from 1.958 Å for the cubic case to 1.996, 1.917, and 2.138 Å for the orthorhombic variant) perpendicularly arranged with respect to the Mn atoms. The long bonds can be regarded as rotated $90°$ within ab on going from one Mn to the neighboring Mn.[3]

When LaMnO$_3$ is in the AF state there are three possible magnetic arrangements according to interplane and intraplane couplings within the [001] plane. (i) With interplane AF coupling and intraplane F coupling the A-AF structure arises. (ii) The opposite structure of A-AF, where the interplane coupling is F and the intraplane coupling AF, is called C-AF structure. In the C-type cell all atoms have two F and four AF nearest neighbors, whereas the reverse is true for A-AF. (iii) If both the inter- and intraplane couplings are AF, the G-AF structure should arise. In the G-type AF lattice, each Mn atom is surrounded by six Mn neighbors whose spins are antiparallel to the chosen central atom. Among the several possible magnetic orderings, the experimental studies show that for LaMnO$_3$ the A-AF ordering is the ground state with a Neeel temperature of 140 K.

The total neutron diffraction was used to identify the crystal structure and lattice parameters of La$_{0.7}$Sr$_{0.3}$MnO$_3$ as well as La$_{0.7}$Ca$_{0.3}$MnO$_3$ and La$_{0.8}$Ca$_{0.2}$MnO$_3$ by Hibble et al.[86] as a function of temperature. LSMO crystallizes in
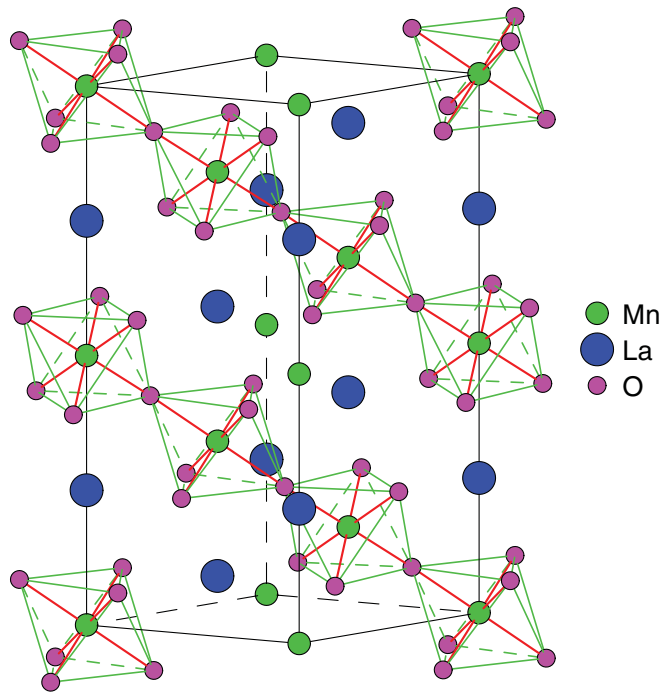
FIG. 2. (Color online) Schematic representation of the rhombo-hedral ($R\bar{3}ch$)-type crystal structure of LSMO.

the rhombohedral ($R\bar{3}ch$, No. 167) crystal structure. The structural parameters used in the calculations are equal to[86] $a = 5.50421$ Å, $b = 5.50421$ Å, and $c = 13.35104$ Å, and atom positions La in $6a$ (0 0 0.25), Mn in $6b$ (0 0 0), Sr in $6a$ (0 0 0.25), and O in $18e$ (0.458 0 0.25). Figure 2 shows the unit cell for the LSMO. In our calculations of the electronic structure of the $La_{0.75}Ca_{0.25}MnO_3$ we used a double cell.

The optical and magneto-optical Kerr spectra have been investigated for perovskite-type hole-doped oxides $La_{1-x}Sr_xMnO_3$ ($x = 0.0$, 0.25) in the photon energy range between 0.92 and 5.8 eV at room temperature. The optical reflectance and transmittance of the samples were measured over a broad energy range from the far infrared through the ultraviolet. To extract the optical constants of the alloys, we used a Drude-Lorentz model. From the parameters obtained, we computed the optical constants, such as the frequency-dependent optical conductivity and the diagonal components of the dielectric tensor. The polar Kerr rotation θ and ellipticity η spectra were measured with a MO spectrometer based on the polarization modulation technique.[87] The angle of incidence of the light on the sample surface mounted inside the 1.5-T water-cooled electromagnet was 3°. The setup was also used to measure θ and η hysteresis loops at fixed light wavelength. The sensitivity of the MO spectrometer is the order 10^{-4}–10^{-5} degrees. The off-diagonal components of the dielectric tensor were calculated by analyzing Kerr rotation, ellipticity, and the determined diagonal elements of the dielectric tensor.

III. RESULTS AND DISCUSSION

A. LaMnO₃

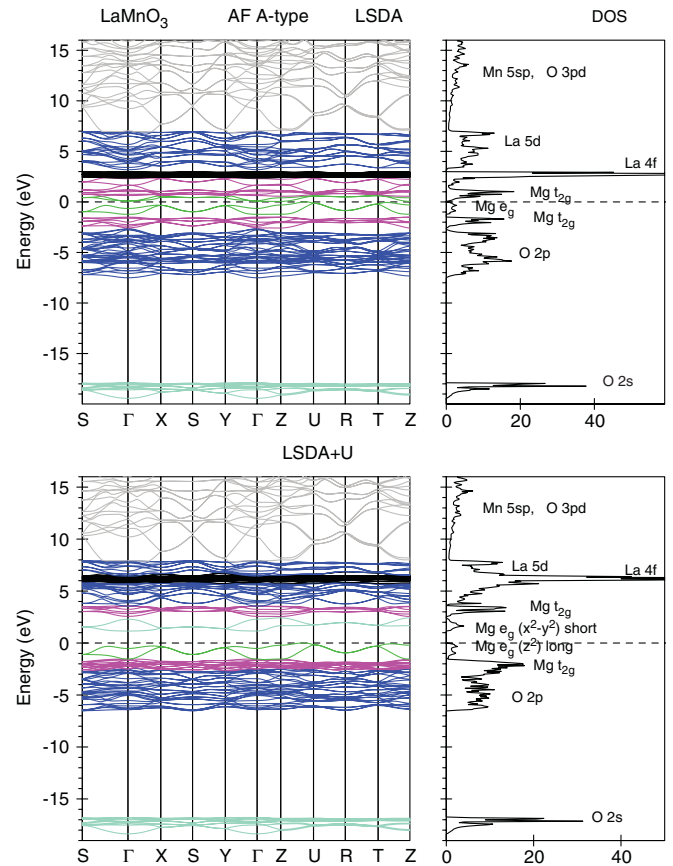The energy band structure and total density of states (DOS) of LaMnO₃ obtained from the fully relativistic LSDA

FIG. 3. (Color online) Fully relativistic spin-polarized LSDA and LSDA + U energy band structures and total DOS [in states/(cell eV)] of LaMnO₃ perovskite for the *Pbmn* structure.

calculations are presented in Fig. 3 both in the LSDA and the LSDA + U approximations for the orthorhombic *Pbnm* structure and *A-AF* ordering. The results agree well with previous band structure calculations.[42–44,50,51] The O 2s states are located mostly between -19.4 and -17.9 eV below the Fermi level and the 2s states of the O are found between -7.5 and -2.7 eV and separated from the 2s bands by an energy gap of about 10.4 eV. The width of the O 2p band is about 4.8 eV. The Mn^{3+} ions have the $t_{2g}^3 e_g^1$ electron configuration in LMO. In cubic LMO crystal structure e_g ($3z^2 - r^2$, $x^2 - y^2$) orbitals are degenerated and situated at the Fermi level in the LSDA calculations. The t_{2g} states due to the crystal field splitting are situated 2 eV lower in energy and well hybridized with O 2p states. A cooperative JT distortion removes the degeneracy of the e_g orbitals and stabilizes the $3d_{3z^2-r^2}$ with respect to the $3d_{x^2-y^2}$ orbitals. The LSDA able to produce correct *A-AF* insulating ground state of LMO in agreement with previous LSDA band structure calculations.[42–44] The highest region can be characterized as La 5d bands from 3.3 to 7.0 eV separated by small energy gap from the La 4f bands. Above this energy interval a mixture of the Mn 5s, Mn 5p, O 3p, and O 3d empty states are situated. The LSDA calculations place the 4f states of La in LaMnO₃ at 2.4 to 3.0 eV above the Fermi level. It is well known that LSDA usually gives a wrong energy position for the 4f states in rare-earth compounds. For nonzero 4f occupation it places the 4f states right at

the Fermi level[88,89] in contradiction with various experimental observations. In the case of La compounds the LSDA places empty $4f$ states too close to the Fermi energy. For example, the LSDA calculations produce the empty $4f$ states in pure La metal at the 2.7 eV above the Fermi level,[90] although according to the BIS measurements they are situated around 5.5 eV above the Fermi level.[91,92]

To put the La empty $4f$ energy states in right position we used the rotationally invariant LSDA $+ U$ method[83] (see lower panel of Fig. 3). We used $U = 5.0$ and $J = 0.92$ eV for the Mn metal site and $U = 6.6$ eV and $J = 0.6$ eV for the La site. In the LSDA $+ U$ band structure calculations occupied on-site Mn $3d$ levels shifted downward by $U_{\text{eff}}/2$ and unoccupied levels shifted upward by this amount; for La $4f$ empty states are shifted upward by the $U_{\text{eff}}/2$ amount. In such an approximation the La $4f$ empty states are situated around 6.3 eV above the Fermi level just in the middle of the La $5d$ states.

The unusual orbital degree of freedom in the manganites originates from the singly occupied degenerate e_g states (d_{3z^2-1} and $d_{x^2-y^2}$) of the Mn^{3+} $3d$ electrons in the $t_{2g}^3 e_g^1$ configuration due to the ligand-field splitting and strong Hund's coupling. This orbital degeneracy makes the Mn^{3+} ion JT active: The degeneracy can be split via biaxial distortion of the surrounding oxygen octahedron. As can be seen from the LSDA $+ U$ calculations the occupied part of the e_g states has the d_{3z^2-1} orbital symmetry and empty e_g states are of the $d_{x^2-y^2}$ orbital symmetry (see bottom panel of Fig. 3).

Loa *et al.* studied LaMnO$_3$ by synchrotron x-ray diffraction, optical spectroscopies, and transport measurements under pressures up to 40 GPa.[93] The pronounced cooperative Jahn-Teller distortion and the GdFeO$_3$-type distortion (octahedral tilting) decrease with increasing pressure. Extrapolation of the data suggests all Mn-O bond lengths become nearly equal around 18 GPa. This equalization of the Mn-O distances means that the cooperative JT effect is reduced with increasing pressure. They infer that the JT effect and the concomitant orbital order are completely suppressed at 18 GPa. On the other hand, the system remains insulating to $\sim$32 GPa where it undergoes a bandwidth-driven insulator-metal transition.

Figure 4 presents Mn d partial DOSs of LaMnO$_3$ with different degree of distortion of the MnO$_6$ octahedra. There is almost perfect orbital ordering in real orthorhombic crystal structure with different Mn-O$_1$ and Mn-O$_2$ interatomic distances (top panel of Fig. 4). Mn e_g states are split by the orthorhombic component of the ligand field into occupied d_{3z^2-1} and empty $d_{x^2-y^2}$ states. These orbitals correspond to long (d_{3z^2-1}) and short ($d_{x^2-y^2}$) Mn-O bond lengths. The occupation number of the d_{3z^2-1} states which lie below the Fermi level reaches the 92% in orthorhombic crystal structure. With decreasing of the distortion of the MnO$_6$ octahedra the mixing of two the orbitals is increased. For the ideal cubic crystal structure with equal Mn-O distances of 1.958 Å the orbital ordering is almost vanished in agreement with the experimental measurements.[93]

The band gap estimated from our LSDA DOS studies for A-AF state is equal to 0.08 eV, this value is smaller than the value of 0.24 eV obtained from resistivity measurements by Mahendiran *et al.*[94] and 0.15 eV reported by Jonker.[95] On the other hand, our LSDA $+ U$ calculations give an energy gap equal to 1.15 eV, which is larger than the experimental
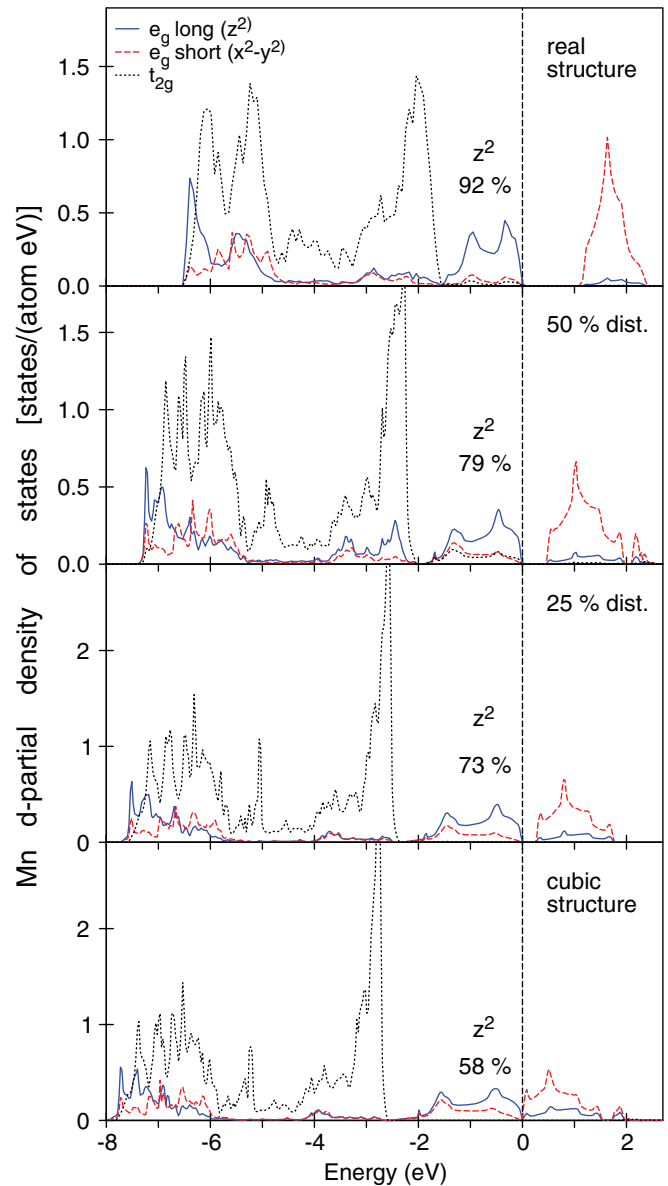

FIG. 4. (Color online) The symmetry separated LSDA $+ U$ Mn d partial density of states [in states/(atom eV)] of LaMnO$_3$ for the orthorhombic GdFeO$_3$-type structure (top panel), artificial cubic structure (bottom panel) and different distortions of the MnO$_6$ octahedra.

measurements. It is also useful to compare our calculated band gap with other theoretical results. The LSDA and LSDA $+ U$ calculations of Yang *et al.*,[50] who used the LMTO-ASA method, gave direct band gaps of 0.1 and 1.0 eV, respectively. The $U + GW$ approach[55] yielded a band gap of 1.6 eV. Pickett and Singh[42] using the LAPW method for the distorted LMO caused by the JT effect obtained a gap of 0.12 eV for the A-type antiferromagnet. The FPLAPW calculations by Ravindran *et al.*[44] produced an energy gap of 0.278 eV. Hence, our LSDA band gap is somewhat smaller than that of other LSDA calculations; on the other hand, our LSDA $+ U$ gap is larger than gaps arising from other LSDA $+ U$ calculations and smaller than the $U + GW$ results.[55]
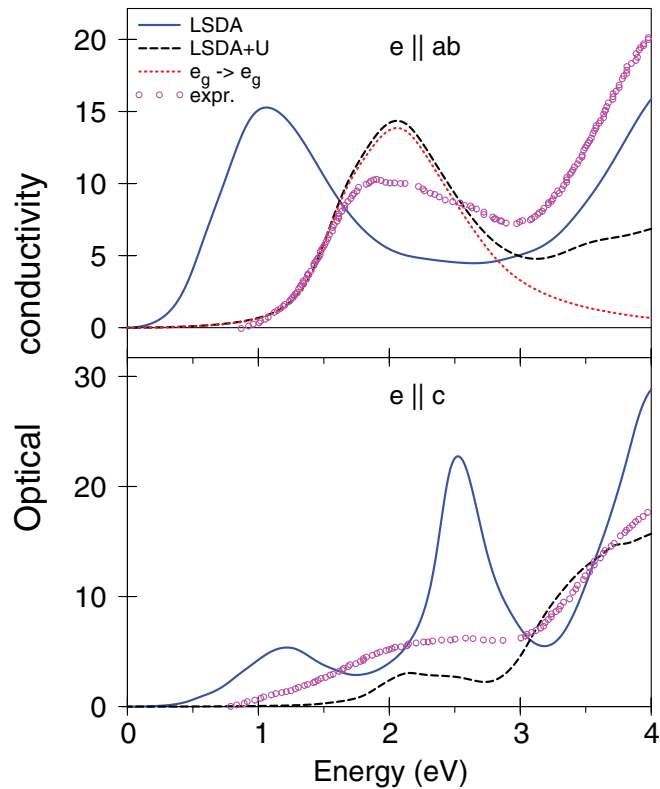
FIG. 5. (Color online) Comparison between experimental diagonal optical conductivity σ_{xx}^1 spectra (circles) of LaMnO$_3$ (Ref. [29]) (in $10^3 \Omega^{-1}$ cm^{-1}) for $\mathbf{E} \perp c$ (top) and $\mathbf{E} \parallel c$ (bottom) and the spectra calculated by the SPR LMTO method in the LSDA (solid line) and the LSDA + U (dashed line) approximations. The dotted line in the top panel presents the theoretically calculated spectrum that occurred between occupied and empty Mn 3d e_g states.

A more precise value of the energy gap may be obtained from the spectroscopy measurements such as optical absorption or photoelectron emission. In such experiments a direct energy gap is measured. The optical[29] and photoemission[96] measurements give direct energy gaps equal to 1.2 and 1.5 eV, respectively. Our calculations produce the corresponding gap as 0.6 and 1.45 eV for the LSDA and LSDA + U calculations, respectively. The later result is in good agreement with the experimental measurements.[96]

Let us compare our calculations with optical measurements. Tobe *et al.*[29] investigated anisotropic optical conductivity and reflectivity spectra for a single crystal of LMO. Jung *et al.*[25] measured reflectivity spectra of LMO in a wide photon energy region between 5 meV and 30 eV at room temperature. Figure 5 shows the comparison between experimentally measured[29] and theoretically calculated optical conductivity spectra for $\mathbf{E} \perp c$ and $\mathbf{E} \parallel c$ light polarization in the ir energy range. Both spectra show prominent peaks around 2 eV. To understand the microscopic origin of the prominent peak at 2 eV in LaMnO$_3$ we performed the decomposition of the calculated σ_{xx}^1 spectrum into the contributions arising from separate interband transitions. As can be seen from Fig. 5 (top panel) the peak around 2 eV is completely determined by the intra-atomic transitions between JT-split Mn^{3+} e_g bands [$(3z^2 - r^2) \rightarrow (x^2 - y^2)$] (see Fig. 3). The transition around
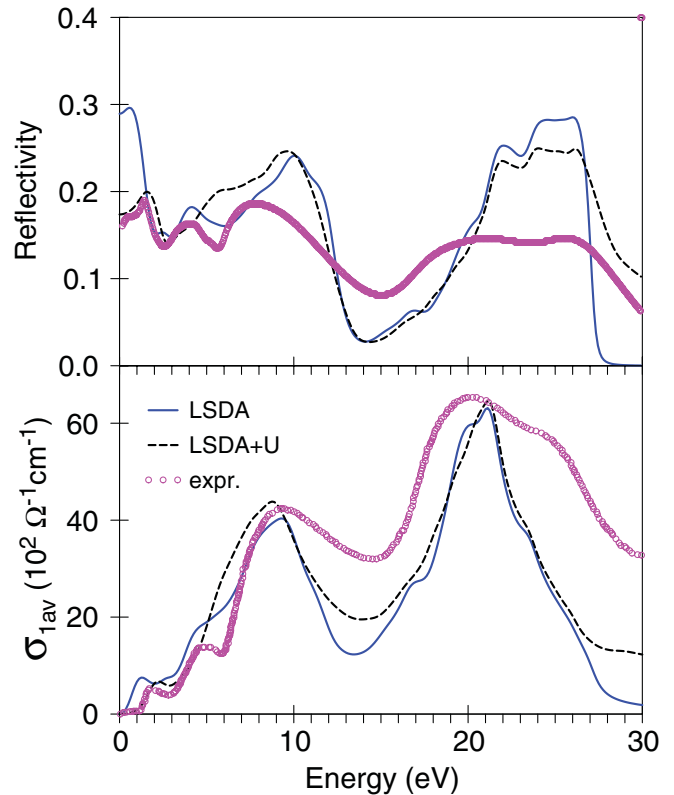

FIG. 6. (Color online) Comparison between experimental optical reflectivity R and diagonal optical conductivity σ_{xx}^1 (circles) of LaMnO$_3$ (Ref. [25]) and the spectra calculated by the LSDA (solid line) and the LSDA + U (dashed line) approximations.

2 eV shows a clear anisotropy for the polarizations parallel and perpendicular to the c axis. The theoretical calculations reproduce well the relative intensity of the prominent peak for the $\mathbf{E} \perp c$ and $\mathbf{E} \parallel c$ polarizations. Due to the underestimation of the energy gap the LSDA calculations place the peak at around 1 eV lower than the experimentally measured spectrum. On the other hand, the LSDA + U approach with $U = 5$ eV gives excellent agreement in the energy position of the peak.

Figure 6 shows the comparison between experimentally measured[25] and theoretically calculated optical conductivity and reflectivity spectra for LaMnO$_3$ in a wide energy interval. The LSDA + U approach well describes the spectra in the ir energy range 0 to 3 eV, while the plain LSDA calculations give slightly better agreement with the experiment for the energies above 3 eV. We can conclude that the LSDA produces reasonably well a description of the quasiparticle interaction in the valence band of LaMnO$_3$ except the small energy range near the Fermi level where the strong Coulomb interaction has to be taken into account.

To explain the microscopic origin of the optical and MO properties of LaMnO$_3$ in terms of individual electronic transitions, we performed the decomposition of the calculated σ_{xx}^1 spectrum into the contributions arising from separate interband transitions (Fig. 7). The optical conductivity spectrum consists of four major peaks labeled as a, b, c, and d. The peak d possesses a high-energy shoulder f. As discussed above, the first peak a around 2 eV is completely determined by the intra-atomic transitions between JT-split Mn^{3+} e_g bands
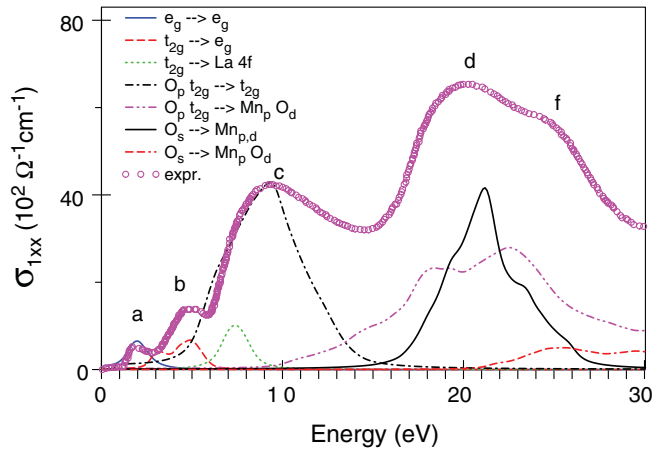
FIG. 7. (Color online) Contributions of different interband transitions to the absorptive part of the diagonal optical conductivity σ_{xx}^1 of LaMnO$_3$ in the LSDA $+ U$ approach compared with the experimental data[25] (open circles).

$[(3z^2 - r^2) \rightarrow (x^2 - y^2)]$. The next feature at 4.5 eV comes from interband transitions between the Mn^{3+} t_{2g} states and the e_g ones [with the $(x^2 - y^2)$ symmetry]. The peak c arises from the O$_p$ and Mn^{3+} $t_{2g} \rightarrow$ Mn^{3+} t_{2g} transitions with an additional contribution from the Mn^{3+} $t_{2g} \rightarrow$ La $4f$ transitions, which contribute to the low-energy part of the peak c. The peak d occupied the wide energy range from 7 to 30 eV and were mostly determined by the O $2p$ and Mn^{3+} $t_{2g} \rightarrow$ Mn $4p$ and O d transitions as well as the more narrow O $2p \rightarrow$ Mn $4pd$ transitions. The shoulder f situated at 26 eV originates from the corresponding peak of the O $2p$ and Mn^{3+} $t_{2g} \rightarrow$ Mn $4p$ and O d transitions. The O $2p$ and $\rightarrow$ Mn $4p$ and O $3d$ transitions contribute to the optical conductivity spectrum above 25 eV.

B. La$_{1-x}$Sr$_x$MnO$_3$

After consideration of the electronic structure and optical spectra of pure LaMnO$_3$ we turn to the doped alloys La$_{1-x}$Sr$_x$MnO$_3$. Optical and magneto-optical Kerr spectra have been investigated for perovskite-type hole-doped oxide La$_{1-x}$Sr$_x$MnO$_3$ ($x = 0.25$) in the photon energy range between 0.92 and 5.8 eV at room temperature. We also calculate the electronic structure, optical and MO spectra of the alloy La$_{0.75}$Sr$_{0.25}$MnO$_3$ using a double unit cell of the rhombohedral ($R3\bar{c}h$) crystal structure (see Fig. 2). The Mn atoms in a double unit cell has two nonequivalent positions, Mn$_1$ and Mn$_2$. The crystal field at the Mn$_1$ site (S_6 point symmetry) splits Mn d states into single a_g ($3z^2 - 1$) state and two double e_g (xy, yz, xz, and $x^2 - y^2$) states. The crystal field at the Mn$_2$ site (C_i point symmetry) splits Mn d states into five single a_g ($xxy, yz, xz, 3z^2 - 1, xz$, and $x^2 - y^2$) states. Figure 8 presents the symmetry separated LSDA partial density of states of La$_{0.75}$Sr$_{0.25}$MnO$_3$ for the rhombohedral ($R3\bar{c}h$) crystal structure.

Our LSDA calculations produce a metallic solution for the La$_{0.75}$Sr$_{0.25}$MnO$_3$ alloy (see Fig. 8). In the metallic phase, the conduction band consists of $3d$ e_g states near the Fermi level, while the t_{2g} electrons are hybridized strongly with the O $2p$ state and localized well below the Fermi level. One should
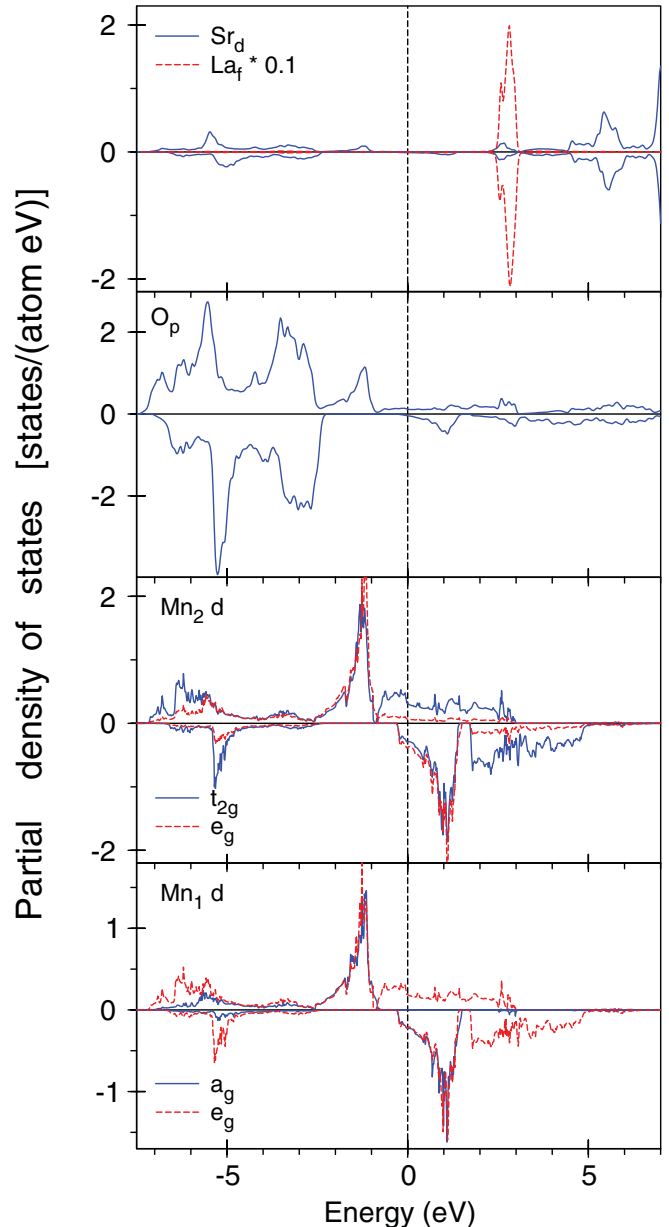

FIG. 8. (Color online) The symmetry-separated LSDA partial density of states [in states/(atom eV)] of La$_{0.75}$Sr$_{0.25}$MnO$_3$ for the rhombohedral ($R3\bar{c}h$) crystal structure.

note that the LSDA gives quite small polarization on the Fermi level in contradiction with the experiment.[1,2] To increase the electron polarization we have to include in our calculation strong Coulomb repulsion through the LSDA $+ U$ approach. In these calculations we used relatively small value of Hubbard $U = 1.85$ eV and exchange parameter $J = 0.92$ eV. The electron polarization is increased from 0.2 for the LSDA to 0.7 for the LSDA $+ U$ calculations. To get a half-metallic solution with vanishing DOS in the minority spin channel we need to apply $U = 2.2$ eV in the case of La$_{0.75}$Sr$_{0.25}$MnO$_3$ alloy.

Figure 9 shows the experimentally measured diagonal optical conductivity σ_{xx} spectra of La$_{0.75}$Sr$_{0.25}$MnO$_3$ and the spectra calculated by the SPR LMTO method in the LSDA and the LSDA $+ U$ ($U = 1.85$ eV) approximations. The experimental σ_{xx}^1 spectrum has low energy minimum at
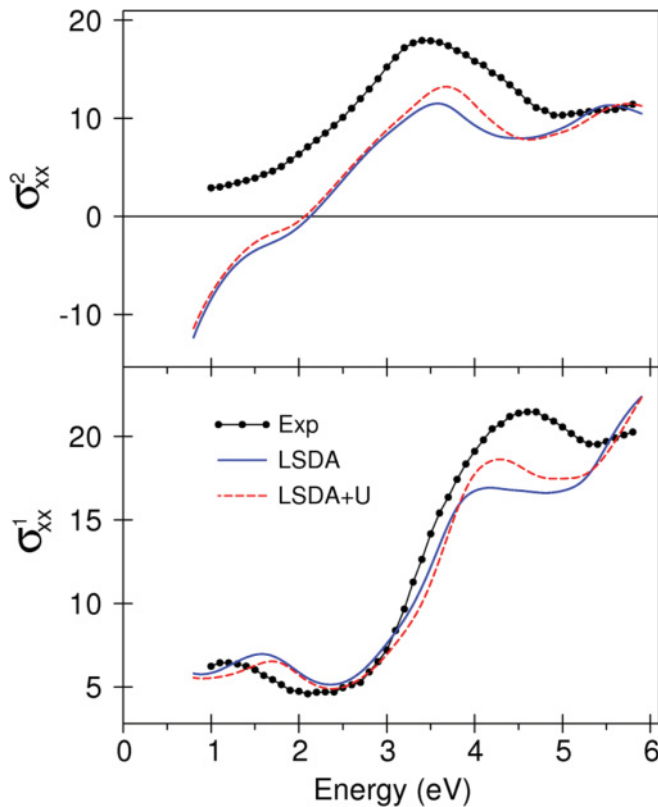
FIG. 9. (Color online) Comparison between the experimental (circles) diagonal optical conductivity σ_{xx} spectra (in 10^{15} s^{-1}) of La$_{0.75}$Sr$_{0.25}$MnO$_3$ and the spectra calculated by the SPR LMTO method in the LSDA (solid lines) and the LSDA $+ U$ (dashed lines) approximations.
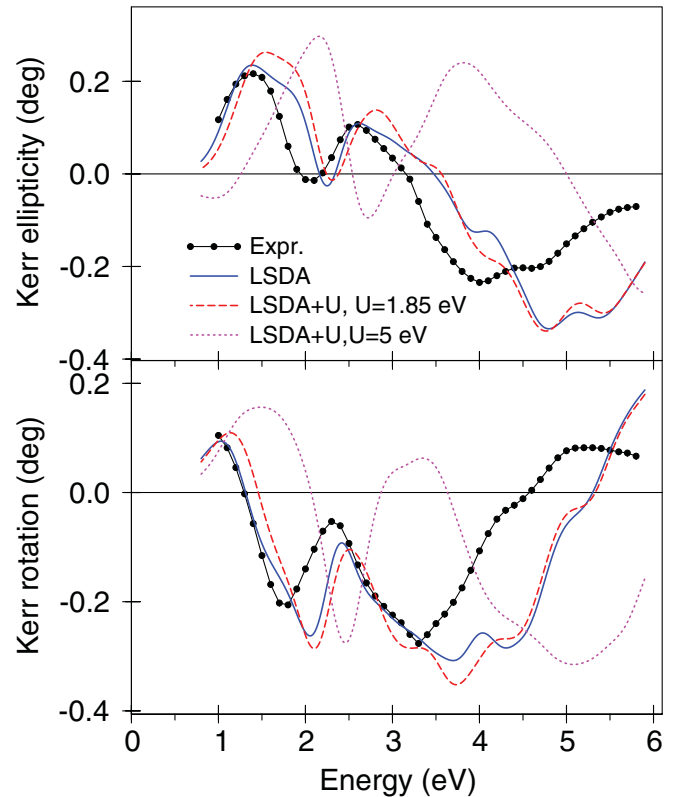

FIG. 10. (Color online) Comparison between the experimental (circles) polar Kerr rotation and ellipticity spectra (in degrees) of La$_{0.75}$Sr$_{0.25}$MnO$_3$ and the spectra calculated by the SPR LMTO method in the LSDA (solid lines) and the LSDA $+ U$ ($U = 1.85$ eV) (dashed lines) and the LSDA $+ U$ ($U = 5$ eV) (dotted lines) approximations.

around 1.2 eV and maximum at 4.6 eV. The LSDA calculations give reasonable agreement in the energy position of the both fine structures; however, the high-energy peak has a red shift in theory of about 0.5 eV. The LSDA theory also underestimates the intensity of the high-energy peak. The LSDA $+ U$ gives a slightly better description for the energy position of the high-energy peak and its intensity; however, there is still 0.35 eV disagreement in their position.

The theoretical curve of the σ_{xx}^2 demonstrates zero crossing (i.e., screened plasma frequency) at around 2 eV, while the experimental curve is expected to have zero crossing at lower energy. One should mention that the theoretically calculated plasma frequencies are usually higher than the experimentally measured ones.[73] In real crystals with different kinds of defects and imperfections the effective masses are larger than the masses for the ideal crystal without imperfections. Therefore, using the perfect crystal approximation leads to the overestimation of the plasma frequency in comparison with the experiment.

The experimentally measured MOKE spectra of the La$_{0.75}$Sr$_{0.25}$MnO$_3$ alloy measured in the magnetic field of 1.5 T (circles) are compared to the corresponding theoretically calculated spectra in the LSDA (solid lines) and LSDA $+ U$ (dashed lines) approximations in Fig. 10. The characteristic features of the measured La$_{0.75}$Sr$_{0.25}$MnO$_3$ Kerr rotation spectrum are two negative minima at around 1.7 and 3.2 eV, a prominent peak at $\sim$2.3 eV, and a broad positive maximum

at around 4.9 eV with a low-energy shoulder at 4.4 eV. The essential points of the experimental Kerr ellipticity spectrum are the zero crossings at 1.7 and 3.2 eV (that correspond to two negative peaks positions in the Kerr rotation), with negative and positive structures between them and a broad negative minimum at the energy of $\sim$1.4 eV with a high-energy shoulder at around 4.4 eV. A narrow positive peak is observed in the Kerr ellipticity at $\sim$1.3 eV that coincides with the Kerr rotation zero crossing at the same energy. The agreement between the experimental and calculated polar Kerr rotation and ellipticity spectra in the vis-uv spectral range is reasonably good. In the energy region below $\sim$3 eV the experimental Kerr ellipticity spectrum agrees well with the calculated one using the LSDA approach both in the shape and the amplitude (Fig. 10). In particular, the energy position and the magnitude of the positive peaks at 1.3 and 2.6 eV are very well reproduced. However, the LSDA as well as the LSDA $+ U$ calculations fail to produce the correct energy position and zero crossing in the high-energy region above 3.5 eV.

One should mention that the use of the Hubbard $U = 5$ eV, which was needed to get the right energy gap in pure LaMnO$_3$ (see previous section), gives completely an inadequate description of the MOKE spectra of the La$_{0.75}$Sr$_{0.25}$MnO$_3$ alloy. We can conclude that the Coulomb correlations are reduced in transition from LMO to LSMO. The carriers in La$_{0.75}$Sr$_{0.25}$MnO$_3$ may be more itinerant than in pure LaMnO$_3$
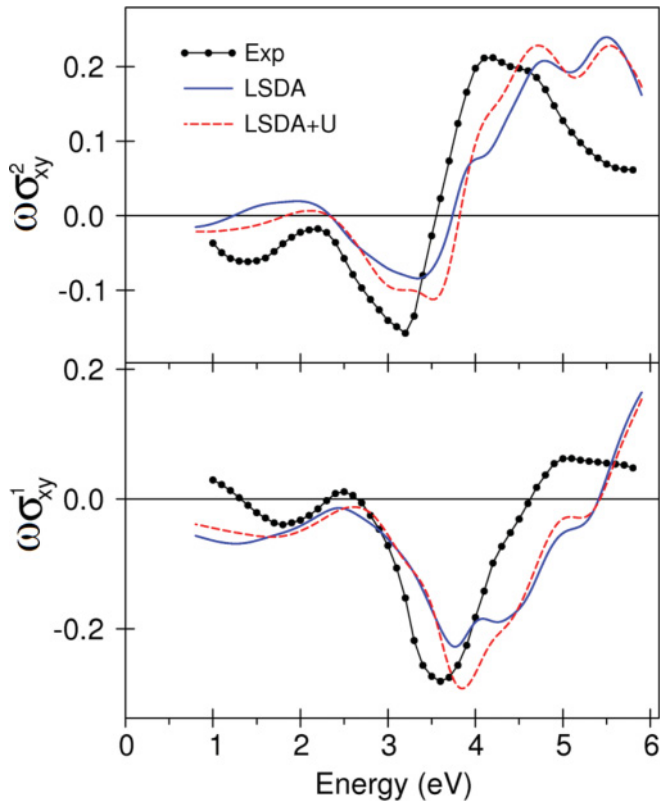
FIG. 11. (Color online) Comparison between the experimental (circles) off-diagonal optical conductivity $\omega\sigma_{xy}$ spectra (in 10^{29} s^{-2}) of La$_{0.75}$Sr$_{0.25}$MnO$_3$ and the spectra calculated by the SPR LMTO method in the LSDA (solid lines) and the LSDA $+ U$ ($U = 1.85$ eV) (dashed lines) approximations.

oxide, due to the increased hybridization between the Mn $3d$ and O $2p$ states.

The interpretation of the MOKE spectra in terms of electronic transitions is a nontrivial task because the complex Kerr rotation is a rather complicated function of both the diagonal and the off-diagonal components of the optical conductivity tensor [Eq. (6)]. Figure 11 presents the comparison between the theoretically calculated and the experimentally estimated off-diagonal parts of the conductivity tensor. The experimental spectra have been obtained from the measured MOKE spectra and the ellipsometry measured complex index of refraction (n and k). In the energy region below ~ 3 eV the experimental $\omega\sigma_{xy}(\omega)$ spectra agree well with the calculated ones using the LSDA approach in both the shape and the amplitude (Fig. 11). There is a small blue shift of around 0.3 eV of the theoretically calculated spectra in comparison with the experiment for negative prominent structures at 3 to 3.5 eV in the $\omega\sigma_{xy}^1(\omega)$ and the $\omega\sigma_{xy}^2(\omega)$. The LSDA $+ U$ approach ($U = 1.85$ eV) gives a slightly better agreement in the energy position and amplitude for these prominent fine structures. The high-energy part of the theoretically calculated spectra exhibits noticeable discrepancies from the experiment both in the LSDA $+ U$ and the LSDA calculations. The theoretically calculated spectra are shifted toward higher energy in comparison with the experiment. One of the possible reasons for such disagreement might be the absence of the dynamical screening effects in our

calculations. The LSDA as well as the LSDA $+ U$ methods are static approaches and miss the effects of dynamical screening. Such effects can be introduced by GW approximation,[63] which is based on the many-electron perturbation theory and treats the screening effects by the dynamical polarization. Nohara *et al.*[53,55] show that the inclusion of the dynamical screening effects may strongly affect the bandwidths, but sometimes in different ways. For example, they show[55] that the width of the majority Mn d t_{2g} band in the energy region between -2.3 and -0.1 eV becomes narrower but the majority Mn $d_{3z^2-r^2}$ band in the energy region between -1.0 and 0 eV becomes broader in $U + GWA$ in comparison with the LSDA $+ U$ results. Therefore, one has to apply the $U + GW$ method for the direct calculation of the optical and MO spectra of LSMO to understand the importance of the dynamical screening effects. Such calculations are highly desired.

IV. SUMMARY

The electronic structure and optical spectra of LaMnO$_3$ oxide have been investigated using the spin-polarized relativistic LMTO method within the spin-DFT as well as with the LSDA $+ U$ approach. A cooperative JT distortion removes the degeneracy of the e_g orbitals in the $t_{2g}^3 e_g^1$ electron configuration of the Mn^{3+} ions and stabilizes the $3d_{3z^2-r^2}$ with respect to the $3d_{x^2-y^2}$ orbitals. It is the origin of so-called A-type antiferromagnetism below $T_N = 140$ K, in which spins align parallel in the xy plane and antiparallel along the z direction. The LSDA is able to produce the correct A-AF insulating ground state in LMO; however, to obtain the correct energy gap and right position of ir peak in the optical conductivity spectrum at 2 eV one has to take into account strong on-site Coulomb correlations through the LSDA $+ U$ approach.

The optical and magneto-optical Kerr spectra have been investigated for perovskite-type hole-doped oxides La$_{1-x}$Sr$_x$MnO$_3$ ($x = 0.25$) in the photon energy range between 0.92 and 5.8 eV at room temperature. The optical reflectance and transmittance of the samples were measured over a broad energy range from the far infrared through the ultraviolet. To extract the optical constants of the alloys, we used a Drude-Lorentz model. From the parameters obtained, we computed the optical constants, such as the frequency-dependent optical conductivity and the diagonal components of the dielectric tensor. The off-diagonal components of the dielectric tensor were calculated by analyzing Kerr rotation, ellipticity, and the determined diagonal elements of the dielectric tensor.

The band structure and MOKE spectra calculations of ferromagnetic La$_{0.75}$Sr$_{0.25}$MnO$_3$ have been performed by the SPR LMTO method. The calculations reproduce the experimentally observed La$_{0.75}$Sr$_{0.25}$MnO$_3$ MOKE spectra in a reasonable way.

The main conclusion drawn by the comparison between experimentally measured and theoretically calculated optical and MOKE spectra is as follows: The electrons in close vicinity of the Fermi level are strongly correlated. To produce the correct energy gap in the LaMnO$_3$ or right value of electron polarization at the Fermi level in ferromagnetic metallic La$_{1-x}$Sr$_x$MnO$_3$ doped alloys one has to take into account strong Coulomb correlations. On the other hand, the electronic

structure and optical and MOKE spectra can be described satisfactorily in terms of the LSDA energy bands beyond close vicinity of the Fermi level. The Coulomb correlations are reduced in transition from LMO to LSMO (from $U = 5.0$ eV to 1.85 eV, respectively). The increased itinerancy of carriers in LSMO can provide some more screening of the bare Coulomb interaction; however, it probably cannot change the Coulomb U so dramatically. We would like to point out that the LSDA $+ U$ method works reasonably well in LaMnO$_3$, giving a correct insulating, AF, and orbital ordering ground state solution. However, it works much worse for LSMO (see Figs. 9–11, where some of the sign changes of the experiment spectra are barely captured by the LSDA $+ U$ approach). The LSDA $+ U$ method which combines LSDA with a basically static, that is, Hartree-Fock-type, mean-field approximation for a multiband Anderson lattice model does not contain true many-body physics. This method can split the lower Hubbard band and higher Hubbard band but it cannot describe the band renormalization resulted from many-body effects. It can be considered only as the first step toward a better description of strongly correlated electron systems. Correct description of the electronic structure and MO properties of the LSMO definitely requires a treatment that goes beyond a static mean-field approximation and includes dynamical effects, for example, the frequency dependence of the self-energy.

[1] G. H. Jonker and J. H. van Santen, Physica **16**, 337 (1950).

[2] E. O. Wollan and W. C. Coehler, Phys. Rev. **100**, 545 (1950).

[3] J. B. Goodenough, Phys. Rev. **100**, 564 (1955).

[4] M. Imada, A. Fujimori, and Y. Tokura, Rev. Mod. Phys. **70**, 1039 (1998).

[5] M. Mochizuki and M. Imada, New J. Phys. **6**, 154 (2004).

[6] E. Dagotto, in *Nanoscale Phase Separation and Colossal Magnetoresistance* (Springer, New York, 2002).

[7] A. Asamitsu, Y. Tomioka, H. Kuwahara, and Y. Tokura, Nature (London) **388**, 50 (1997).

[8] M. Fiebig, K. Myano, Y. Tomioka, and Y. Tokura, Science **280**, 1925 (1998).

[9] M. Salamon and M. Jaime, Rev. Mod. Phys. **73**, 583 (2001).

[10] N. Sakai, H. Fjellvig, and B. Lebech, Acta Chem. Scand. **51**, 904 (1997).

[11] C. Ritter, M. R. Ibarra, J. M. De Teresa, P. A. Algarabel, C. Marquina, J. Blasco, J. Garcia, S. Oseroff, and S.-W. Cheong, Phys. Rev. B **56**, 8902 (1997).

[12] J. Rodriguez-Carvajal, M. Hennion, F. Moussa, A. H. Moudden, L. Pinsard, and A. Revcolevschi, Phys. Rev. B **57**, 3189 (1998).

[13] E. O. Wollan and W. C. Koehler, Phys. Rev. **100**, 545 (1955).

[14] B. C. Hauback, H. Fjellvag, and N. Sakai, J. Solid State Chem. **124**, 43 (1996).

[15] N. Furukawa, J. Phys. Soc. Jpn. **63**, 3214 (1994).

[16] A. J. Millis, P. B. Littlewood, and B. I. Shraiman, Phys. Rev. Lett. **74**, 5144 (1995).

[17] A. J. Millis, R. Mueller, and B. I. Shraiman, Phys. Rev. B **54**, 5405 (1996).

[18] C. M. Varma, Phys. Rev. B **54**, 7328 (1996).

[19] L. F. Feiner and A. M. Oles, Phys. Rev. B **59**, 3295 (1999).

[20] S. Jin, T. Tiefel, M. McCormack, R. Fastnacht, R.Ramesh, and L. Chen, Science **264**, 413 (1994).

[21] Y. Tokura, A. Urushibara, Y. Moritomo, A. Asamitsu, G. Kido, and N. Furukawa, J. Phys. Soc. Jpn. **63**, 418 (1994).

[22] C. Zener, Phys. Rev. **82**, 403 (1951).

[23] P. G. de Gennes, Phys. Rev. **118**, 141 (1960).

[24] T. Arima and Y. Tokura, J. Phys. Soc. Jpn. **64**, 2488 (1995).

[25] J. H. Jung, K. H. Kim, D. J. Eom, T. W. Noh, E. J. Choi, J. Yu, Y. S. Kwon, and Y. Chung, Phys. Rev. B **55**, 15489 (1997).

[26] Y. Okimoto, T. Katsufuji, T. Ishikawa, T. Arima, and Y. Tokura, Phys. Rev. B **55**, 4206 (1997).

[27] S. Yoon, H. L. Liu, G. Schollerer, S. L. Cooper, P. D. Han, D. A. Payne, S. W. Cheong, and Z. Fisk, Phys. Rev. B **58**, 2795 (1998).

[28] K. Takenaka, K. Iida, Y. Sawaki, S. Sugai, Y. Moritomo, and A. Nakamura, Phys. Status Solidi **215**, 637 (1999).

[29] K. Tobe, T. Kimura, Y. Okimoto, and Y. Tokura, Phys. Rev. B **64**, 184421 (2001).

[30] A. S. Moskvin, A. A. Makhnev, L. V. Nomerovannaya, N. N. Loshkareva, and A. M. Balbashov, Phys. Rev. B **82**, 035106 (2010).

[31] A. S. Moskvin and R. V. Pisarev, Low Temp. Phys. **36**, 489 (2010).

[32] N. N. Kovaleva, A. M. Oles, A. M. Balbashov, A. Maljuk, D. N. Argyriou, G. Khaliullin, and B. Keimer, Phys. Rev. B **81**, 235130 (2010).

[33] P. Fumagalli, C. Spaeth, G. Guenterodt, R. Helmholt, and J. Wecker, IEEE Trans. Magn. **31**, 3277 (1995).

[34] S. Yamaguchi, Y. Okimoto, K. Ishibashi, and Y. Tokura, Phys. Rev. B **58**, 6862 (1998).

[35] T. J. A. Popma and M. G. J. Kamminga, Solid State Commun. **17**, 1073 (1975).

[36] T. Ogasawara, M. Matsubara, Y. Tomioka, M. Kuwata-Gonokami, H. Okamoto, and Y. Tokura, Phys. Rev. B **68**, 180407 (2003).

[37] N. N. Loshkareva, E. A. Gan'shina, B. I. Belevtsev, Y. P. Sukhorukov, E. V. Mostovshchikova, A. N. Vinogradov, V. B. Krasovitsky, and I. N. Chukanova, Phys. Rev. B **68**, 024413 (2003).

[38] M. Koubaa, A. Haghiri-Gosnet, J. Renard, M. Veis, V. Kolinsky, S. Visnovsky, P. Lecoeur, W. Prellier, and B. Mercey, J. Magn. Magn. Mater. **272–276**, 1812 (2004).

[39] R. Rauer, G. Neuber, J. Kunze, J. Bäckström, M. R. bhausen, T. Walter, and K. Dörr, J. Magn. Magn. Mater. **290-291**, 948 (2005).

[40] J. Mistrika, T. Yamaguchi, M. Veis, E. Liskova, S. Visnovsky, M. Koubaa, A. M. Haghiri-Gosnet, P. Lecoeur, J. P. Renard, W. Prellier *et al.*, J. Appl. Phys. **99**, 08Q317 (2006).

[41] D. D. Sarma, N. Shanthi, S. R. Barman, N. Hamada, H. Sawada, and K. Terakura, Phys. Rev. Lett. **75**, 1126 (1995).

[42] W. E. Pickett and D. J. Singh, Phys. Rev. B **53**, 1146 (1996).

[43] D. J. Singh and W. E. Pickett, Phys. Rev. B **57**, 88 (1998).

[44] P. Ravindran, A. Kjekshus, H. Fjellvag, A. Delin, and O. Eriksson, Phys. Rev. B **65**, 064445 (2002).

[45] S. Gong and B. G. Liu, Phys. Lett. A **375**, 1477 (2011).

[46] B. R. K. Nanda and S. Satpathy, J. Magn. Magn. Mater. **322**, 3653 (2010).

[47] B. R. K. Nanda and S. Satpathy, Phys. Rev. B **81**, 174423 (2010).

[48] S. Satpathy, Z. S. Popovic, and F. R. Vukajlovic, Phys. Rev. Lett. **76**, 960 (1996).

[49] I. Solovyev, N. Hamada, and K. Terakura, Phys. Rev. B **53**, 7158 (1996).

[50] Z. Yang, Z. Huang, L. Ye, and X. Xie, Phys. Rev. B **60**, 15674 (1999).

[51] W. Y. Hu, M. C. Qian, Q. Q. Zheng, H. Q. Lin, and H. K. Wong, Phys. Rev. B **61**, 1223 (2000).

[52] C. Ma, Z. Yang, and S. Picozzi, J. Phys.: Condens. Matter **18**, 7717 (2006).

[53] Y. Nohara, A. Yamasaki, S. Kobayashi, and T. Fujiwara, Phys. Rev. B **74**, 064417 (2006).

[54] T. Kotani and H. Kino, J. Phys.: Condens. Matter **21**, 266002 (2009).

[55] Y. Nohara, S. Yamamoto, and T. Fujiwara, Phys. Rev. B **79**, 195110 (2009).

[56] K. Held, O. K. Andersen, M. Feldbacher, A. Yamasaki, and Y. F. Yang, J. Phys.: Condens. Matter **20**, 064202 (2008).

[57] T. Hashimoto, S. Ishibashi, and K. Terakura, Phys. Rev. B **82**, 045124 (2010).

[58] R. Maezono, S. Ishihara, and N. Nagaosa, Phys. Rev. B **58**, 11583 (1998).

[59] A. E. Bocquet, T. Mizokawa, T. Saitoh, H. Namatame, and A. Fujimori, Phys. Rev. B **46**, 3771 (1992).

[60] J. Inoue and S. Maekawa, Phys. Rev. Lett. **74**, 3407 (1995).

[61] T. Geng, Z. Z. Han, and S. L. Zhuang, Physica B **405**, 3714 (2010).

[62] K. Held and D. Vollhardt, Phys. Rev. Lett. **84**, 5168 (2000).

[63] L. Hedin, Phys. Rev. A **139**, 796 (1965).

[64] H. Liu, K. Y.-J. Zhang, L. Wu, L. Uba, S. Uba, W. Chang, J.-Y. Lin, and L. Wang, J. Magn. Magn. Mater. **304**, e303 (2006).

[65] W. H. Kleiner, Phys. Rev. **142**, 318 (1966).

[66] M. I. Friezer, IEEE Trans. Magn. **4**, 152 (1968).

[67] J. B. Kortright and S.-K. Kim, Phys. Rev. B **62**, 12216 (2000).

[68] W. Reim and J. Schoenes, in *Ferromagnetic Materials*, edited by E. P. Wohlfarth and K. H. J. Buschow (North-Holland, Amsterdam, 1990), Vol. 5, p. 133.

[69] J. Schoenes, in *Electronic and Magnetic Properties of Metals and Ceramics*, edited by R. W. Cahn, P. Haasen, and E. J. Kramer, Materials Science and Technology, Vol. 3A (Verlag Chemie, Weinheim, 1992).

[70] R. Kubo, J. Phys. Soc. Jpn. **12**, 570 (1957).

[71] C. S. Wang and J. Callaway, Phys. Rev. B **9**, 4897 (1974).

[72] V. N. Antonov, A. I. Bagljuk, A. Y. Perlov, V. V. Nemoshkalenko, V. N. Antonov, O. K. Andersen, and O. Jepsen, Low Temp. Phys. **19**, 494 (1993).

[73] V. Antonov, B. Harmon, and A. Yaresko, *Electronic Structure and Magneto-optical Properties of Solids* (Kluwer, Dordrecht, 2004).

[74] L. Uba, S. Uba, V. N. Antonov, A. N. Yaresko, and R. Gontarz, Phys. Rev. B **64**, 125105 (2001).

[75] L. Uba, S. Uba, V. N. Antonov, A. N. Yaresko, T. Slezak, and J. Korecki, Phys. Rev. B **62**, 13731 (2000).

[76] V. N. Antonov, L. Uba, S. Uba, A. N. Yaresko, A. Y. Perlov, and V. V. Nemoshkalenko, Low Temp. Phys. **27**, 425 (2001).

[77] L. Uba, A. Polewko, S. Uba, R. Gontarz, A. N. Yaresko, and V. N. Antonov, Phys. Status Solidi A **196**, 145 (2003).

[78] O. K. Andersen, Phys. Rev. B **12**, 3060 (1975).

[79] V. V. Nemoshkalenko, A. E. Krasovskii, V. N. Antonov, V. N. Antonov, U. Fleck, H. Wonn, and P. Ziesche, Phys. Status Solidi B **120**, 283 (1983).

[80] U. von Barth and L. Hedin, J. Phys. C **5**, 1629 (1972).

[81] P. E. Blöchl, O. Jepsen, and O. K. Andersen, Phys. Rev. B **49**, 16223 (1994).

[82] V. I. Anisimov, J. Zaanen, and O. K. Andersen, Phys. Rev. B **44**, 943 (1991).

[83] A. N. Yaresko, V. N. Antonov, and P. Fulde, Phys. Rev. B **67**, 155103 (2003).

[84] G. Matsumoto, J. Phys. Soc. Jpn. **29**, 606 (1970).

[85] J. B. A. A. Elemans, B. V. Laar, K. R. V. D. Veen, and B. O. Looptra, J. Solid State Chem. **3**, 238 (1971).

[86] S. J. Hibble, Cooper, S. P. Hannon, A. C. Fawcett, and I. D. Greenblatt, J. Phys.: Condens. Matter **11**, 9221 (1999).

[87] K. Sato, Jpn. J. Appl. Phys. **20**, 2403 (1981).

[88] V. N. Antonov, B. N. Harmon, and A. N. Yaresko, Phys. Rev. B **63**, 205112 (2001).

[89] V. N. Antonov, B. N. Harmon, and A. N. Yaresko, Phys. Rev. B **66**, 165208 (2002).

[90] W. E. Pickett, A. J. Freeman, and D. D. Koelling, Phys. Rev. B **22**, 2695 (1980).

[91] J. Lang, Y. Baer, and P. Cox, J. Phys. F **11**, 121 (1981).

[92] Y. Baer and W. D. Schneider, in *Handbook of the Physics and Chemistry of Rare Earths*, edited by K. A. Gschneidner, L. Eyring, and S. Hüfner (North-Holland, Amsterdam, 1987), Vol. 10, p. 1.

[93] I. Loa, P. Adler, A. Grzechnik, K. Syassen, U. Schwarz, M. Hanfland, G. K. Rozenberg, P. Gorodetsky, and M. P. Pasternak, Phys. Rev. Lett. **87**, 125501 (2001).

[94] R. Mahendiran, S. K. Tiwary, A. K. Raychaudhuri, T. V. Ramakrishnan, R. Mahesh, N. Rangavittal, and C. N. R. Rao, Phys. Rev. B **53**, 3348 (1996).

[95] G. H. Jonker, Physica (Amsterdam) **20**, 1118 (1954).

[96] T. Saitoh, A. E. Bocquet, T. Mizokawa, H. Namatame, A. Fujimori, M. Abbate, Y. Takeda, and M. Takano, Phys. Rev. B **51**, 13942 (1995).